

Modified full bridge dual inductive coupling resonant converter for electric vehicle battery charging applications

Kondreddy Sreekanth Reddy, Sreenivasappa Bhupasandra Veeranna

Center for Research in Power Electronics, Presidency University, Bengaluru, India

Article Info

Article history:

Received Jul 23, 2021

Revised Feb 28, 2022

Accepted Mar 10, 2022

Keywords:

Constant current mode

Constant voltage mode

Electric vehicle

Inductive coupling resonant converter

Integrated converter

Isolation

ABSTRACT

In this paper, a modified full bridge dual inductive coupling (LCL) resonant converter for electric vehicles (EVs) battery charging applications is proposed. The main objective of the proposed topology is to operate the converter in constant voltage (CV) and constant current (CC) mode during battery charging. The presented topology's uniqueness comprises the following: i) isolated charging and power factor correction (PFC), ii) to achieve zero-voltage switching (ZVS) and zero-current switching (ZCS) for inverter switches, iii) reduction of number of rectifier diodes to reduce the conduction and switching losses, and iv) reducing the magnetizing current. The output voltage dependence of resonant converter is reduced using a PFC converter against the variations of the alternating current (AC) grid input voltage. The variations of the wide range output voltage and load is compensated by a small variation in switching frequency. The proposed topology's detailed operation is simulated using the MATLAB/Simulink tool.

This is an open access article under the [CC BY-SA](https://creativecommons.org/licenses/by-sa/4.0/) license.



Corresponding Author:

Kondreddy Sreekanth Reddy

Center for Research in Power Electronics, Presidency University

Rajankunte, Yelahanka, Bengaluru, Karnataka-560064, India

Email: ksreekanthreddy@presidencyuniversity.in

1. INTRODUCTION

The demand for electric vehicles (EVs) and plug-in hybrid electric vehicles (PHEVs) is ever increasing due to an impending scarcity of fossil fuels is expected. and the zero emission of carbon dioxide (CO₂), noise reduction, smooth functioning, and high efficiency. The power electronic converters in EVs and PHEVs play a significant role in interfacing the battery and grid to drive the traction motor which are discussed in [1]–[5]. The design of reliable, compact and efficient power electronic converters is of great interest and challenge for the researchers and engineers [6]–[8].

Presently, many topologies have been proposed in the literature for isolated battery charging using inductors capacitor (LLC) resonant converters [9]–[22]. The topologies proposed in reference [9]–[17] describes the operation of direct current/alternating current (DC/AC) and AC/DC converter for battery charging with high frequency transformer to achieve isolation during charging. Hu *et al.* [9] a modified LLC converter with two transformers in series is proposed for wide input voltage range. Based on the input voltage, a scheme is developed to reduce the magnetizing current by modifying the magnetising inductance adaptively while keeping high DC voltage gain. However, the topology needs two extra switches and four diodes which eventually leads to conduction loss as well as control complexity in operating extra switches. Dusmez and Khaligh [10], by incorporating the resonant inductor inside the transformer, the LLC resonant converter's bulk is reduced, making it particularly appropriate for use as an integrated onboard charger for electric vehicles. However, the report gives no indication of the imbalanced leakage inductance that is fairly

prevalent in centre tapped transformers with bifilar windings or the parameter changes that occur when a resonant inductor is used. Wu *et al.* [11] proposes a unique secondary-side phase-shift-controlled LLC resonant converter to decrease magnetising inductance circulating current. The topology is not designed for high DC voltage gain, thus activities like constant voltage (CV) charge, constant current (CC) charge, zero-voltage switching (ZVS), and zero-current switching (ZCS) are not reported. To eliminate low and high frequency current ripple on the battery a new resonant tank for an LLC resonant DC-DC converter is proposed in [12] considering only half bridge inverter which doesn't guarantee high DC voltage gain. Though, peak to peak low frequency voltage ripple of 0.14 V is achieved but the peak to peak low frequency current ripple is limited to 0.537 A only. An LLC resonant DC-DC converter design procedure is presented in reference [13] for an onboard lithium-ion battery charger of a PHEV. Based on fundamental harmonic approximation (FHA) the worst-case circumstances for primary-side ZVS operation are identified analytically and charging profile is implemented considering a constant maximum power (CMP). To ensure soft-switching throughout the operation, worst-case operating point is used. To avoid the inaccuracy of FHA approach below the resonance region, based on specific operation mode the design constraints are explained briefly. In order to validate the designed equations only full bridge LLC resonant converter is considered which doesn't guarantee high DC voltage gain or high DC current gain. Deng *et al.* [14], a dual-bridge LLC resonant converter for wide input voltage range is proposed and a fixed frequency pulse width modulation (PWM) control scheme is employed. The magnetising inductor limits the voltage gain range regardless of the quality factor. In addition to this, two extra switches in the topology increases the cost and control complexities. An LLC resonant converter is proposed in reference [15] with considerable resonant inductance in order to form an adjustable wide-range regulated voltage source. Soft switching is employed by properly choosing the dead time and maximum switching frequency for power switches under inductive region operating conditions. A frequency control strategy is used for the proposed topology to handle wide regulated output voltages against wide input voltage or output load variations. A novel dual full-bridge LLC (FBLLC) resonant converter for implementing CC and CV charges is proposed in reference [16]. The paper quickly explains ZVS for all primary switches in CV charge and approximately ZCS for all primary switches in CC charge. Both CC and CV charge consider fixed frequency resonant operation to limit circulating current. To get high DC voltage gain, the article includes an extra diode bridge, and which results in greater conduction losses. However, the proposed topology is claimed to be operated at fixed switching frequency for both CC and CV operations, although clarity on how same switching frequency may be used for two different resonant frequencies is lacking. This is significant because when the resonance frequency is lower than the switching frequency, the active switches of the inverter suffer from excessive turn-off current, when it is greater, and the main side of the transformer suffers from circulating current. To operate a lower resonant converter in CC charge mode, turn off the switch connected in series with an extra capacitor, and turn on the switch to lower the resonant frequency. This contradicts the paper's CC and CV charge operational point of view. Moreover, while the switch is off, the circuit lacks a discharge pathway for the added capacitor, resulting heating and a deficit of current restriction. Besides the aforesaid, the suggested topology's closed loop control approach lacks clarity on selecting a common proportional-integral (PI) controller for both CV and CC charges. The paper also fails to describe the resonant converter's output voltage dependence on the ac grid input voltage.

In the present paper, a modified full bridge LCL resonant converter topology is proposed to address the afore-mentioned issues. The proposed topology comprises of power factor correction (PFC) converter and an isolated full bridge dual-inductive coupling converter (FBD-LCL) is briefly explained in the next section. The organization of the paper is being as: in section 2, the description of the proposed topology is explained along with various modes of operation. Section 3 discusses, the control techniques used for the proposed topology. In section 4 design analysis are included. The simulation results are included in section 5 and the conclusion are outlined in section 6.

2. DESCRIPTION OF THE PROPOSED TOPOLOGY

The proposed modified FBD-LCL converter topology is shown in Figure 1 includes an active switch S_b , an inductor L_1 , a diode D_5 and a capacitor C_2 in PFC converter, four active switches (S_1 – S_4) constitutes full bridge inverter with body diodes (D_6 – D_9), two resonant converters upper and lower. The upper resonant converter composed of L_{r1} , C_{r1} , and L_{m1} . The lower resonant converter composed of L_{r2} , L_{r3} , C_{r2} , L_{m2} , and a switch S_r . The diode bridge rectifier with four diodes (D_{10} – D_{13}) at secondary of the transformer and a filter capacitor C_3 .

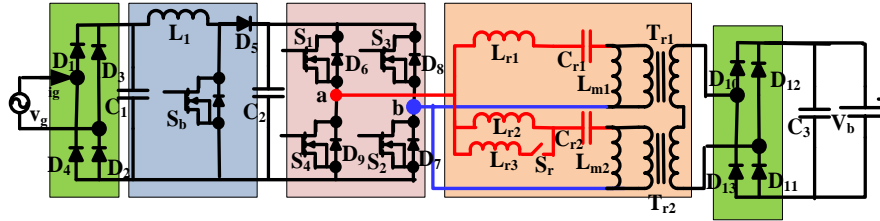


Figure 1. Proposed modified full bridge dual LCL resonant converter

2.1. Power factor correction converter

The PFC converter is the first stage in EVs and PHEVs charging system designed to provide power factor correction. As per international electrotechnical commission (IEC) 1000-3-2 standard, it is mandatory to limit the harmonic current drawn by the charging system to low, which is measured through total harmonic distortion (THD) and to generate input current waveform close to sinusoidal. In addition to this, when the converter operates at high switching frequency to achieve higher power density, increasing the efficiency, and reducing the electro-magnetic interference (EMI) is a major concern. The EMI standard EN55022 class B formed to control and eliminate high frequency radiated and conducted EMI which can inject unwanted signals into the neighboring circuits and/or systems [17]–[19]. In order to fulfill the requirements of the above standards, boost converter is used as PFC converter in the proposed topology due to its simplicity and reduced size of the filter. The PFC converter, in addition to perform power factor correction function it also provides constant DC voltage to the full bridge inverter.

2.2. Operating principle of the proposed converter

The proposed converter consists of two LCL resonant converters, upper resonant converter FBD-LCL₁, and lower resonant converter FBD-LCL₂. The operating principle of proposed converter is explained through full bridge LCL resonant converter based on FHA method as shown in Figure 2 to Figure 5. Each LCL resonant converter operates at two different resonant frequencies, upper resonant frequency (f_{ru}) and lower resonant frequency (f_{rl}). The resonant converter is operated as constant voltage source at f_{ru} as in (1) and is operated as constant current source at f_{rl} as in (2).

$$f_{ru} = \frac{1}{2\pi\sqrt{L_r C_r}} \tag{1}$$

$$f_{rl} = \frac{1}{2\pi\sqrt{(L_r + L_m) C_r}} \tag{2}$$

When the resonant converter operates at f_{ru} it behaves as a constant voltage source, the DC voltage gain is obtained based on FHA analysis [6] is given by (3):

$$G_v = \frac{f_x}{n\sqrt{(f_x^2(1+L_i) - L_i)^2 + Q^2(f_x^2 - 1)^2}} \tag{3}$$

Where $G_v = \frac{V_o}{V_{ac}}$ DC voltage gain. Normalized frequency $f_x = \frac{f_s}{f_{ru}}$, f_s is switching frequency. Inductance ratio $L_i = \frac{L_r}{L_m}$. Quality factor $= \frac{Z_o}{R_{ac}}$, $Z_o = \sqrt{\frac{L_r}{C_r}}$ characteristic impedance. $R_{ac} = 0.81 \cdot n^2 \cdot R_o$ is the AC equivalent resistance. $R_o = \frac{V_o}{I_o}$ is the output DC resistance. n is the transformer turns ratio. When the resonant converter operates at f_{rl} it behaves as a constant current source, the output current is obtained as in (4):

$$|I_o(w)| = \frac{V_{ac}}{w \cdot n \left[\{L_r + R_{ac}(L_m + L_r)\} - \left\{ \frac{(1 + R_{ac})}{w C_r} \right\} \right]} \tag{4}$$

where $= 2\pi f_x$, $f_x = \frac{f_s}{f_{rl}}$.

The graph between voltage gain (G_v) versus normalized frequency (f_x) with constant inductor ratio (L_i) of 5 and variable quality factor (Q) is shown in Figure 2. It is very clear from the graph that, as Q increases G_v decreases, at f_{xmin} gain is highest at f_{xmax} gain is lowest and at $f_x = f_s$ gain is unity. The ZVS and ZCS regions are also indicated in the graph. In Figure 3, Gain versus normalized frequency with constant quality factor and current increases at $f_x = f_s$ for increasing value of Q and decreases when $f_x < 1$ or $f_x > 1$.

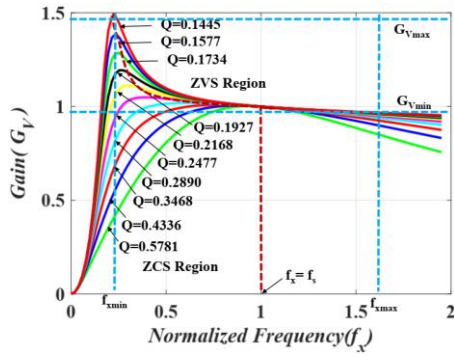


Figure 2. Graph between gain (G_V) versus f_x with constant $L_i = 5$ and variable Q

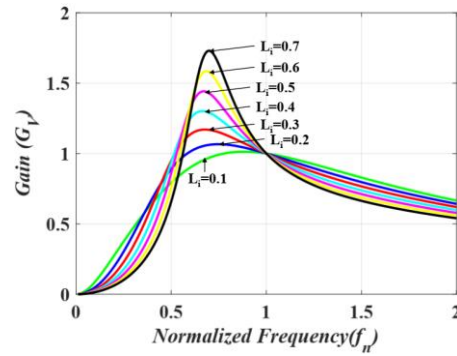


Figure 3. Graph between gain (G_V) versus f_x with constant $Q = 0.7$ and variable L_i

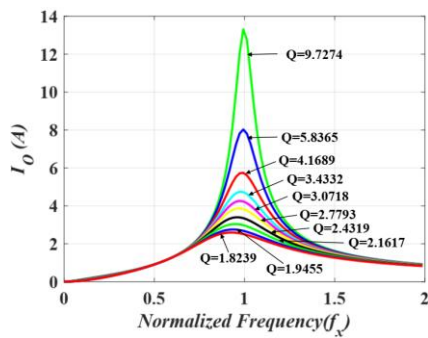


Figure 4. Graph between output current versus f_x with constant $L_i = 2$ and variable Q

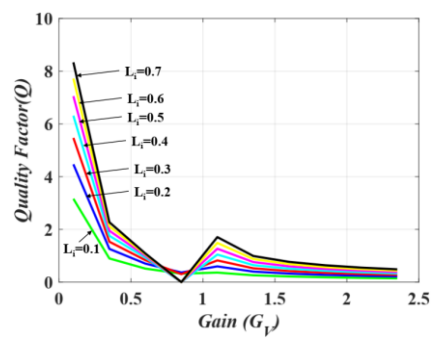


Figure 5. Graph between Q versus Gain (G_V) with variable L_i

2.3. Charge and discharge profile characteristics of the battery

The charge and discharge profile of voltage, current, power and equivalent impedance of EV battery in CC and CV mode are given in Figure 6 and Figure 7 respectively. The voltage varies from a minimum voltage of 220 V to a maximum voltage of 400 V for Li-ion battery which consists of 96 cells. The battery charging operation starts with CC mode with a constant current of 2.5 A and ends when the battery attains a maximum voltage equal to 400 V. Using mode selector switch S_r , the battery charging operation is changed from CC mode to CV charge mode. In CV charge mode, the battery voltage is maintained at constant voltage of 400 V but the current drawn by the battery is decreased from an initial current of 2.5 A to final current of 0.25 A at the end of this mode. It is also clear from charge profile characteristics indicated in Figure 6 (left-figure) that, the FBD-LCL₁ converter is designed to provide constant voltage of 200 V, whereas FBD-LCL₂ converter is designed to provide an initial voltage of 20 V in the beginning of CC charge mode and a final voltage of 200 V at the end of CC charge mode. Both FBD-LCL₁ and FBD-LCL₂ converters are designed to deliver a continuous 200 V to get a battery voltage of 400 V. Figure 6 (right) shows the battery power and impedance during CC/CV charge mode. The initial battery power is 550 W and the final battery power is 1000 W. At the end of CV charge mode, it drops to 100 W. The starting battery impedance is 88 and reaches 160 at the conclusion of CC charge mode, then gradually climbs as the battery current demand drops. The discharge profile characteristics of EV battery is also included in Figure 7, left-figure indicates battery voltage and current and right-figure indicates battery power and impedance during battery discharge.

2.4. Constant current charge mode

In this mode upper resonant converter FBD-LCL₁ behaves as constant voltage source and lower resonant converter FBD-LCL₂ behaves as constant current source. The upper resonant converter FBD-LCL₁ resonate at two frequencies, upper resonant frequency f_{ru1_CCM} as in (5) and lower resonant frequency f_{rl1_CCM} as in (6).

$$f_{ru1_CCM} = \frac{1}{2\pi\sqrt{L_{r1}C_{r1}}} \tag{5}$$

$$f_{ru1_CCM} = \frac{1}{2\pi\sqrt{(L_{r1}+L_{m1})C_{r1}}} \tag{6}$$

In order to operate FBD-LCL₁ converter as constant voltage source, it is operated at upper resonant frequency f_{ru1_CCM} . The lower resonant converter FBD-LCL₂ resonate at two frequencies, upper resonant frequency f_{ru2_CCM} as in (7) and lower resonant frequency f_{rl2_CCM} as in (8).

$$f_{ru2_CCM} = \frac{1}{2\pi\sqrt{(L_{r2}|L_{r3})C_{r2}}} \tag{7}$$

$$f_{rl2_CCM} = \frac{1}{2\pi\sqrt{((L_{r2}|L_{r3})+L_{m2})C_{r2}}} \tag{8}$$

In order to operate FBD-LCL₂ converter as constant current source, it is operated at lower resonant frequency f_{rl2_CCM} .

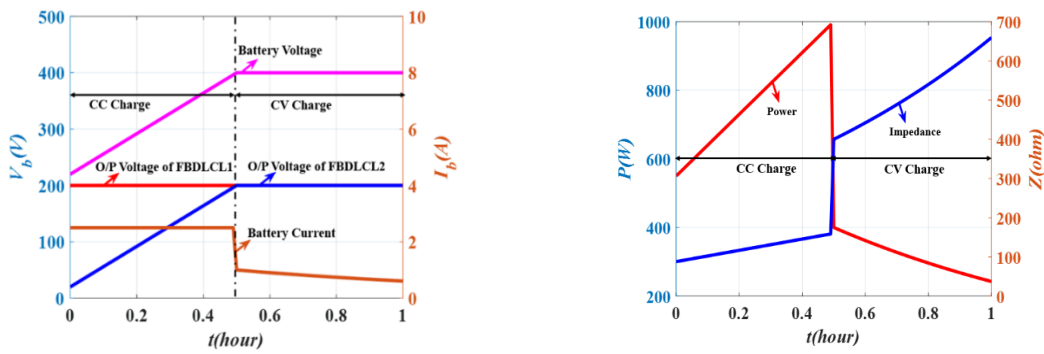


Figure 6. Charge profile characteristics of EV battery during CC/CV charge mode: battery voltage, FBD-LCL₁ converter voltage, FBD-LCL₂ converter voltage (left y-axis) and battery current (right y-axis) in left-figure, battery power (left y-axis), and battery impedance (right y-axis) right-figure

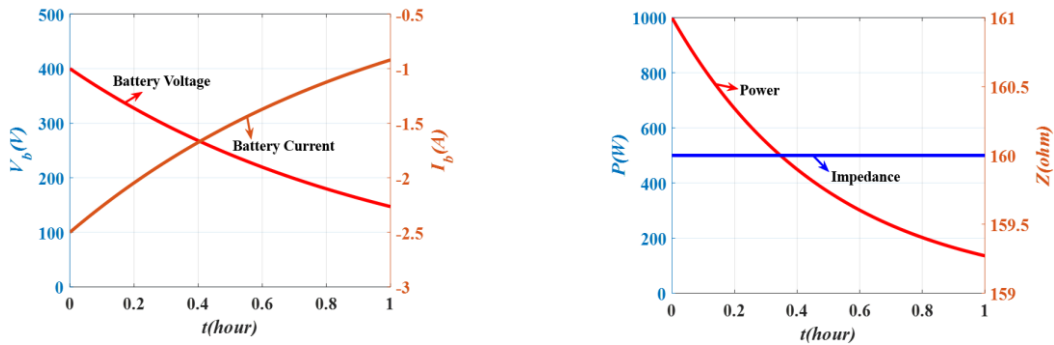


Figure 7. Discharge profile characteristics of EV battery: battery voltage (left y-axis) and battery current (right y-axis) in left-figure, battery power (left y-axis), and battery impedance (right y-axis) in right-figure

2.5. Constant voltage charge mode

In this mode both upper resonant converter FBD-LCL and lower resonant converter FBD-LCL₂ behaves as constant voltage source. The upper resonant converter FBD-LCL₁ resonate at two frequencies, upper resonant frequency f_{ru1_CVM} as in (9) and lower resonant frequency f_{rl1_CVM} as in (10).

$$f_{ru1_CVM} = \frac{1}{2\pi\sqrt{L_{r1}C_{r1}}} \tag{9}$$

$$f_{rl1_CVM} = \frac{1}{2\pi\sqrt{(L_{r1}+L_{m1})C_{r1}}} \tag{10}$$

In order to operate FBD-LCL₁ converter as constant voltage source, it is operated at upper resonant frequency f_{ru1_CVM} . The lower resonant converter FBD-LCL₂ resonate at two frequencies, upper resonant frequency f_{ru2_CVM} as in (11) and lower resonant frequency f_{rl2_CVM} as in (12).

$$f_{ru2_CVM} = \frac{1}{2\pi\sqrt{L_{r2}C_{r2}}} \tag{11}$$

$$f_{rl2_CVM} = \frac{1}{2\pi\sqrt{(L_{r2}+L_{m2})C_{r2}}} \tag{12}$$

In order to operate FBD-LCL₂ converter as constant voltage source, it is operated at upper resonant frequency f_{ru2_CVM} .

3. CONTROL TECHNIQUE

The control technique for the proposed topology to obtain DC link voltage and to charge battery are shown in Figure 8 and Figure 9 respectively. The references [23]–[25] deliberates few governing control techniques used in EV applications for power factor correction. The implementation of CC and CV charge mode of operation needs closed loop control scheme. Hence, the external feedback signals from the DC link voltage, battery voltage, battery current, PFC inductor current, and resonating inductor current are used to choose the control method inputs for the proposed design. The PFC converter and FBD-LCL converter control techniques are concisely presented in the following sections.

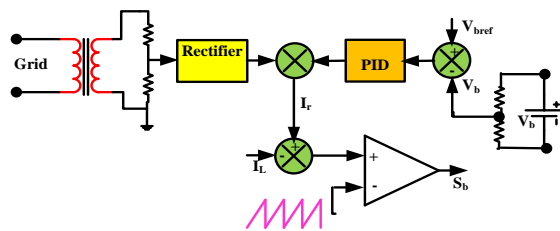


Figure 8. Control technique for PFC converter

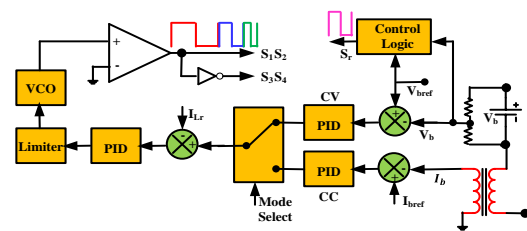


Figure 9. Control technique for FBD-LCL converter

3.1. Power factor correction converter control technique

In Figure 8, the PFC converter is controlled by a PI controller, rectifier, adder/subtractor, and comparator. A transformer and a resistive network are used to reduce the AC grid voltage to the desired level. This AC voltage is rectified and filtered to produce V_r , the reference DC voltage. The error signal is obtained by comparing the reference V_{bref} to the observed V_b . For the regulated step signal, this error signal is sent into the PI controller's reference current input I_r . The step signal is compared to the high frequency saw tooth signal to generate a PWM signal for the switch S_b .

3.2. Full bridge dual-inductive coupling converter converter control technique

The Figure 9 shows three proportional integral derivative (PID) controllers, a mode selector switch, three subtractors, a limiter, a voltage-controlled oscillator (VCO), and a comparator. As long as the battery voltage is below the peak charge voltage, the mode selector switch will activate the current controller to charge the battery. When the battery voltage hits 400 V, the mode selector switch automatically shifts from CC to CV. The error signal from the inner loop PID controller is supplied to the mode selector switch output. The step signal is limited for saturation and then sent to a VCO for variable frequency. The PWM pulses for MOSFET switches S1, S2, S3, and S4 have configurable switching frequency. Simulink auto tuner finds Kp, Ki, and Kd values for all three PIDs.

4. DESIGNING PARAMETERS AND EQUATION

The factors needed to select switches, diodes, resonant circuits whose primary goal is to achieve soft switching conditions across its operating range and passive components are discussed in this section.

4.1. Selection of switches and diodes

The collection of a power semiconductor switches and diodes is based on reverse blocking voltage, maximum forward current, and power handling capabilities. In the proposed topology the inverter module

consists of five MOSFET switches $S_b, S_1, S_2, S_3,$ and S_4 with body diodes and the bridge rectifier circuit is formed with nine additional diodes $D_1-D_5,$ and $D_{10}-D_{13}$ are considered.

4.2. Selection of transformer turns ratio

The transformer turns ratio n is defined as:

$$n = \frac{V_{dc}}{V_o + 2V_D} \quad (13)$$

where V_{dc} is rated input voltage, V_o is rated output voltage and V_D is the forward voltage drop of rectifier diode.

4.3. Selection of resonating elements and magnetizing inductances

The selection of resonating elements inductance, capacitance and magnetizing inductances which are used in Figure 1 for the upper resonant converter elements and the lower resonant converter elements are calculated based on constant current charge and constant voltage charge mode. The equations pertaining to the calculations of these inductances and capacitances are included in (5) to (12).

4.4. Selection of rectifier, direct current-link and battery side capacitors

Three capacitors C_1 at the output of the input bridge rectifier, C_2 at the high DC-link, and C_3 across the battery are used in the proposed converter. The formulas for constructing these capacitors are as shown in:

$$C_1 = \frac{1}{4\sqrt{3}fR_b\gamma} \quad (14)$$

$$C_2 = \frac{V_{DC}}{4f_s R \Delta V_{DC}} \quad (15)$$

$$C_3 = \frac{V_b}{4f_s R_b \Delta V_b} \quad (16)$$

5. RESULTS AND DISCUSSION

The results and discussion of the proposed topology are briefly explained in this section. The simulation of the proposed topology was verified using MATLAB/Simulink version R2019a for the Table 1 specifications. Figures 10 to 14 show the simulation results for power factor correction, switching pulses, inverter voltage and current, ZVS and ZCS operation, transformer primary and secondary voltage and current, and voltage and current through rectifying diodes. To produce the rated output voltage of 400 V, the rectifier stage generates a 380-420 V DC voltage at the output terminal.

The switching and resonant frequencies are 50 kHz. V_{Cr} is the resonant capacitor voltage, V_{DS1} is the drain to source voltage of S_1 , I_{DS1} is the drain to source current via S_1 , v_{D10} , and v_{D12} are voltages and i_{D10} and i_{D12} are currents of rectifier diodes D_{10} and D_{12} respectively. The transformer primary voltage, primary current, secondary voltage and secondary current are v_{P1} , i_{P1} , v_{S1} , i_{S1} respectively.

Figure 10 shows the grid voltage, grid current, DC link voltage, and DC link current waveforms. The measured power factor (PF) is 0.99 with a lower current harmonic distortion (ITHD) of 0.97. Figure 11 shows that ZVS of power switches and ZCS of rectifier diodes were achieved at 400 V output voltage. In Figure 12 switching pulse between gate and source of S_1 , drain to source voltage of S_1 and current through S_1 switch indicating ZVS turn-on and ZCS turn-off conditions are shown. It is very clear from the results that when voltage is zero switch is turned-off and when current is zero switch is turned-on. The transformer primary voltage, primary current, secondary voltage and secondary current are given in Figure 13 and in Figure 14, voltage across and current through rectifier diode D_{10} indicating ZVS turn-on and ZCS turn-off are included. Similar operations can also be performed on other rectifying diodes (D_{11} , D_{12} , and D_{13}) in the secondary side full-bridge rectifier.

Table 1. Parameters and specifications

Parameters	Specifications	Parameters	Specifications
Grid voltage (V_s) and frequency	220 V and 50 Hz	Magnetizing inductance L_{m1} and L_{m2}	127 μ H and 70 μ H
Battery Power (P_b)	1 kW	Resonant capacitor C_{r1} and C_{r2}	79 nF and 24 nF
Battery Voltage (V_b)	220 V - 400 V	Leakage inductance L_{r2}	17 μ H
DC link voltage minimum and maximum (V_{dc_min})	380 V and 420 V	Leakage inductance L_{r3}	27 μ H
Switching frequency (f_s)	50 kHz	Rectifier side capacitor (C_1)	1000 μ F
Turns ratio of T_{r1} and T_{r2} (1:n ₁)	1:0.5	DC link capacitor (C_2)	470 μ F
Leakage inductance L_{r1}	7 μ H	Battery side capacitor (C_3)	220 μ F

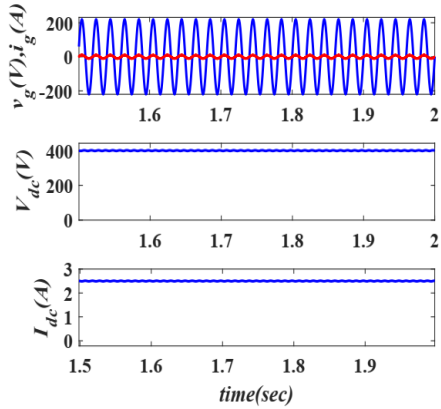


Figure 10. Waveforms of (top)-grid voltage (blue) and grid current (red) with $PF=0.99$, $I_{THD} = 0.99$, (middle)-DC link voltage and (bottom)-DC link current

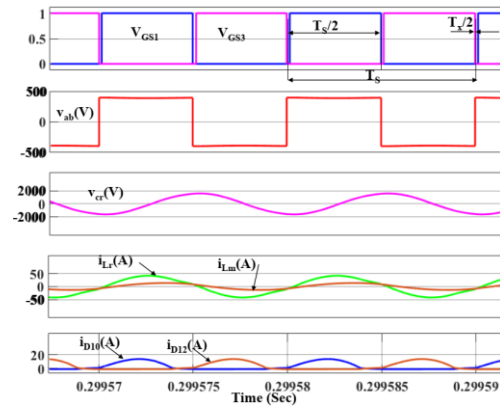


Figure 11. Waveforms of switching pulses, inverter voltage, capacitor voltage, current through inductors L_r and L_m and current through rectifier diodes i_{D10} and i_{D12}

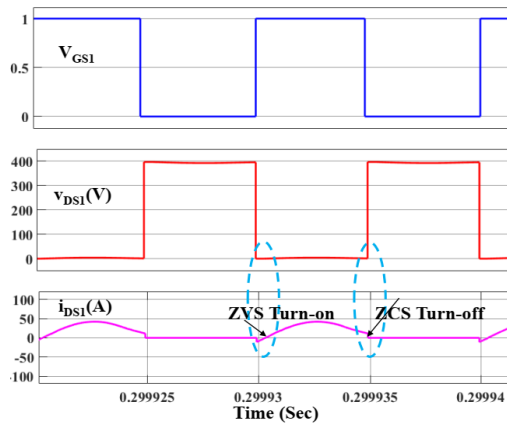


Figure 12. Waveforms of switching pulse applied between gate and source of S_1 , drain to source voltage of S_1 and current through S_1 switch indicating ZVS turn-on and ZCS turn-off

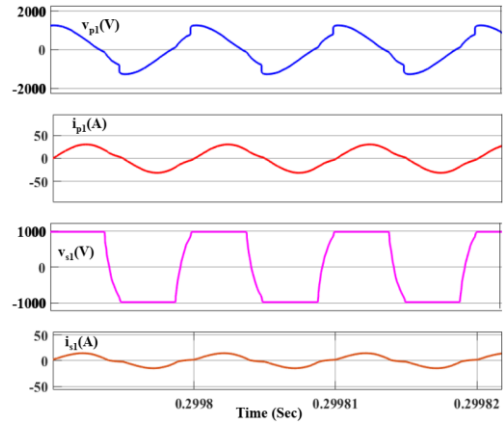


Figure 13. Waveforms of transformer primary voltage, primary current, secondary voltage, and secondary current

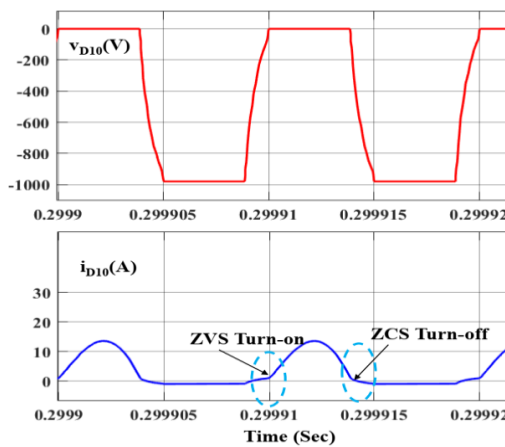


Figure 14. Waveforms of voltage across and current through rectifier diode D_{10} indicating ZVS turn-on and ZCS turn-off

6. CONCLUSION

In this paper a modified full bridge dual LCL resonant converter fit for implementing both CC and CV charge operation for charging the batteries is proposed. The PFC converter is also included in the proposed topology for power factor correction. The implementation of two resonant converters to resonate at lower and upper resonant frequencies, results in ZVS and ZCS of the converter switches in the CC charge and CV charge operations. The ZVS turn-on and ZCS turn-off is also achieved during rectification operation of the converter at the output. The higher resonant frequency is obtained by operating lower resonant converter also in CV charge mode with the help of mode selector switch. The operation of ZVS and ZCS ensure that the converter operates with no switching losses. This will improve the efficiency of the converter over a wide range of output voltage and hence the suggested architecture catches instant applications in battery charging systems of electric vehicles.

REFERENCES

- [1] S. Kumar and A. Usman, "A Review of Converter Topologies for Battery Charging Applications in Plug-in Hybrid Electric Vehicles," *2018 IEEE Industry Applications Society Annual Meeting (IAS)*, 2018, pp. 1–9, doi: 10.1109/IAS.2018.8544609.
- [2] L. Xue, Z. Shen, D. Boroyevich, P. Mattavelli, and D. Diaz, "Dual Active Bridge-Based Battery Charger for Plug-in Hybrid Electric Vehicle with Charging Current Containing Low Frequency Ripple," in *IEEE Transactions on Power Electronics*, vol. 30, no. 12, pp. 7299–7307, December 2015, doi: 10.1109/TPEL.2015.2413815.
- [3] M. Yilmaz and P. T. Krein, "Review of Battery Charger Topologies, Charging Power Levels, and Infrastructure for Plug-In Electric and Hybrid Vehicles," in *IEEE Transactions on Power Electronics*, vol. 28, no. 5, pp. 2151–2169, May 2013, doi: 10.1109/TPEL.2012.2212917.
- [4] M. S. Arifin, N. Mohammad, M. I. Khalil, and M. J. Alam, "Input switched closed-loop single phase ĆUK AC to DC converter with improved power quality," *International Journal of Power Electronics and Drive System (IJPEDS)*, vol. 10, no. 3, pp. 1373–1381, September 2019, doi: 10.11591/ijpeds.v10.i3.pp1373-1381.
- [5] S. M. Rezvanizani, Z. Liu, Y. Chen, and J. Lee, "Review and Recent Advances in Battery Health Monitoring and Prognostics Technologies for Electric Vehicle (EV) Safety and Mobility," *Journal of Power Sources*, vol. 256, pp. 110–124, June 2014, doi: 10.1016/j.jpowsour.2014.01.085.
- [6] W. Srirattana-wichaiikul and P. Wirasant, "Evaluation of lightweight battery management system with field test of electric bus in campus transit system," *International Journal of Electrical and Computer Engineering (IJECE)*, vol. 10, no. 6, pp. 6202–6213, December 2020, doi: 10.11591/ijece.v10i6.pp6202-6213.
- [7] K. Liu, X. Hu, Z. Yang, Y. Xie, and S. Feng, "Lithium-ion Battery Charging Management Considering Economic Costs of Electrical Energy Loss and Battery Degradation," *Energy Conversion and Management*, vol. 195, pp. 167–179, September 2019, doi: 10.1016/j.enconman.2019.04.065.
- [8] J. Hong, H. Lee, and K. Nam, "Charging method for the second battery in dual inverter drive systems for electric vehicles," *2014 IEEE Applied Power Electronics Conference and Exposition-APEC 2014*, 2014, pp. 2407–2414, doi: 10.1109/APEC.2014.6803640.
- [9] H. Hu, X. Fang, F. Chen, Z. J. Shen, and I. Batarseh, "A Modified High-Efficiency LLC Converter with Two Transformers for Wide Input-Voltage Range Applications," in *IEEE Transactions on Power Electronics*, vol. 28, no. 4, pp. 1946–1960, April 2013, doi: 10.1109/TPEL.2012.2201959.
- [10] S. Dusmez and A. Khaligh, "A Compact and Integrated Multifunctional Power Electronic Interface for Plug-in Electric Vehicles," in *IEEE Transactions on Power Electronics*, vol. 28, no. 12, pp. 5690–5701, December 2013, doi: 10.1109/TPEL.2012.2233763.
- [11] H. Wu, T. Mu, X. Gao, and Y. Xing, "A Secondary-Side Phase-Shift-Controlled LLC Resonant Converter with Reduced Conduction Loss at Normal Operation for Hold-Up Time Compensation Application," in *IEEE Transactions on Power Electronics*, vol. 30, no. 10, pp. 5352–5357, October 2015, doi: 10.1109/TPEL.2015.2418786.
- [12] F. Musavi, M. Craciun, D. S. Gautam, W. Eberle, and W. G. Dunford, "An LLC Resonant DC–DC Converter for Wide Output Voltage Range Battery Charging Applications," in *IEEE Transactions on Power Electronics*, vol. 28, no. 12, pp. 5437–5445, December 2013, doi: 10.1109/TPEL.2013.2241792.
- [13] F. Musavi, M. Craciun, D. S. Gautam, and W. Eberle, "Control Strategies for Wide Output Voltage Range LLC Resonant DC–DC Converters in Battery Chargers," in *IEEE Transactions on Vehicular Technology*, vol. 63, no. 3, pp. 1117–1125, March 2014, doi: 10.1109/TVT.2013.2283158.
- [14] J. Deng, S. Li, S. Hu, C. C. Mi and R. Ma, "Design Methodology of LLC Resonant Converters for Electric Vehicle Battery Chargers," in *IEEE Transactions on Vehicular Technology*, vol. 63, no. 4, pp. 1581–1592, May 2014, doi: 10.1109/TVT.2013.2287379.
- [15] X. Sun, X. Li, Y. Shen, B. Wang, and X. Guo, "Dual-Bridge LLC Resonant Converter with Fixed-Frequency PWM Control for Wide Input Applications," in *IEEE Transactions on Power Electronics*, vol. 32, no. 1, pp. 69–80, January 2017, doi: 10.1109/TPEL.2016.2530748.
- [16] R. Beiranvand, B. Rashidian, M. R. Zolghadri, and S. M. H. Alavi, "Using LLC Resonant Converter for Designing Wide-Range Voltage Source," in *IEEE Transactions on Industrial Electronics*, vol. 58, no. 5, pp. 1746–1756, May 2011, doi: 10.1109/TIE.2010.2052537.
- [17] H. Vu and W. Choi, "A Novel Dual Full-Bridge LLC Resonant Converter for CC and CV Charges of Batteries for Electric Vehicles," in *IEEE Transactions on Industrial Electronics*, vol. 65, no. 3, pp. 2212–2225, March 2018, doi: 10.1109/TIE.2017.2739705.
- [18] B. Lu, W. Dong, S. Wang, and F. C. Lee, "High frequency investigation of single-switch CCM power factor correction converter," *Nineteenth Annual IEEE Applied Power Electronics Conference and Exposition, 2004. APEC '04.*, vol. 3, pp. 1481–1487, 2004, doi: 10.1109/APEC.2004.1296060.
- [19] K. S. Reddy and S. B. Veeranna, "Integrated buck and boost converter for a universal battery charger of an Electric Vehicle," *E3S Web of Conferences. EDP Sciences*, vol. 309, p. 01073, September 2021, doi: 10.1051/e3sconf/202130901073.
- [20] K. S. Reddy and S. B. Veeranna, "Single Phase Multifunctional Integrated Converter for Electric Vehicles," *Indonesian Journal of Electrical Engineering and Computer Science*, vol. 24, no. 3, pp. 1342–1353, December 2021, doi: 10.11591/ijeecs.v24.i3.pp1342-1353.

- [21] P. He and A. Khaligh, "Design of 1 kW bidirectional half-bridge CLLC converter for electric vehicle charging systems," *2016 IEEE International Conference on Power Electronics, Drives and Energy Systems (PEDES)*, 2016, pp. 1–6, doi: 10.1109/PEDES.2016.7914445.
- [22] N. Saxena, I. Hussain, B. Singh, and A. L. Vyas, "Implementation of a Grid-Integrated PV-Battery System for Residential and Electrical Vehicle Applications," in *IEEE Transactions on Industrial Electronics*, vol. 65, no. 8, pp. 6592–6601, August 2018, doi: 10.1109/TIE.2017.2739712.
- [23] L. Zhang and X. Ruan, "Control Schemes for Reducing Second Harmonic Current in Two-Stage Single-Phase Converter: An Overview From DC-Bus Port-Impedance Characteristics," in *IEEE Transactions on Power Electronics*, vol. 34, no. 10, pp. 10341–10358, October 2019, doi: 10.1109/TPEL.2019.2894647.
- [24] L. Zhang, X. Ruan, and X. Ren, "Second-Harmonic Current Reduction for Two-Stage Inverter with Boost-Derived Front-End Converter: Control Schemes and Design Considerations," in *IEEE Transactions on Power Electronics*, vol. 33, no. 7, pp. 6361–6378, July 2018, doi: 10.1109/TPEL.2017.2746878.
- [25] L. Zhang, *et al.*, "Design Considerations of High-Voltage-Insulated Gate Drive Power Supply for 10 kV SiC MOSFET in Medium-Voltage Application," *2019 IEEE Applied Power Electronics Conference and Exposition (APEC)*, 2019, pp. 425–430, doi: 10.1109/APEC.2019.8721965.

BIOGRAPHIES OF AUTHORS



Kondreddy Sreekanth Reddy     is an Assistant professor in Electrical and Electronics Engineering Department at Presidency University, Bangalore, Karnataka since 2017. He received his B.Tech from Sri Sai Institute of Technology and Science affiliated to JNTU Hyderabad in 2008, M.Tech in power electronics from VIT University Vellore in 2010 and currently he is pursuing Ph.D. degree in Electrical and Electronics Engineering from Presidency University, Bangalore Karnataka. He worked as an Assistant Professor in Lovely Professional University Punjab from 2010 to 2017. His research interest include power electronics converters for electric vehicles. He can be contacted at email: ksreekanthreddy@presidencyuniversity.in.



Sreenivasappa Bhupasandra Veeranna     is a professor of Electronics and Communication Engineering with the School of Engineering, Presidency University, Bangalore, Karnataka since 2017. He received his B.E. degree in electronics and communication engineering from Dayananda Sagar College of Engineering, Bangalore in 2000, and M.Tech. degree in power electronics from B.M.S. college of engineering, Bangalore in 2005 and Ph.D. degree in electrical engineering from National Institute of Technology Surathkal Karnataka, in 2012. From 2005 to 2012, he was an Assistant and then Associate Professor with Nitte Meenakshi Institute of Technology, Bangalore. From 2010 to 2011, he worked as Visiting Graduate Research Assistant with department of electrical engineering, The Petroleum Institute, Abu Dhabi, UAE. His research interests include power electronics and drives, pulse width modulation techniques, multilevel inverters, electric vehicles, developing high-frequency energy conversion systems to improve the efficiency and performance. He can be contacted at email: sreenivasappabv@presidencyuniversity.in.